Vision-Based Recovery of Unmanned Aerial Vehicles

A.D. Kahn
Tactical Electronic Warfare Division

Introduction: A key requirement for performing reconnaissance missions using small unmanned aerial vehicles (UAVs) from a ship is the ability to automatically recover the air vehicle on board the ship. The automatic landing system must be simple to use, not add additional hardware to the air vehicle, and have a minimal footprint to the operation of the ship.

Current systems used for automatic landing of UAVs on board ships require the installation of large and/or expensive equipment on the air vehicle.[1-3] Some of these systems present a logistics challenge due to their large footprint on board ships.

The system in this program addresses these issues by leveraging the existing reconnaissance payload consisting of a video camera and transmitter, along with the existing UAV autopilot and data link. On the ship, in addition to the UAV operator terminal and hardware, is a laptop computer and recovery target with optical markers. Figure 1 presents the recovery system concept.
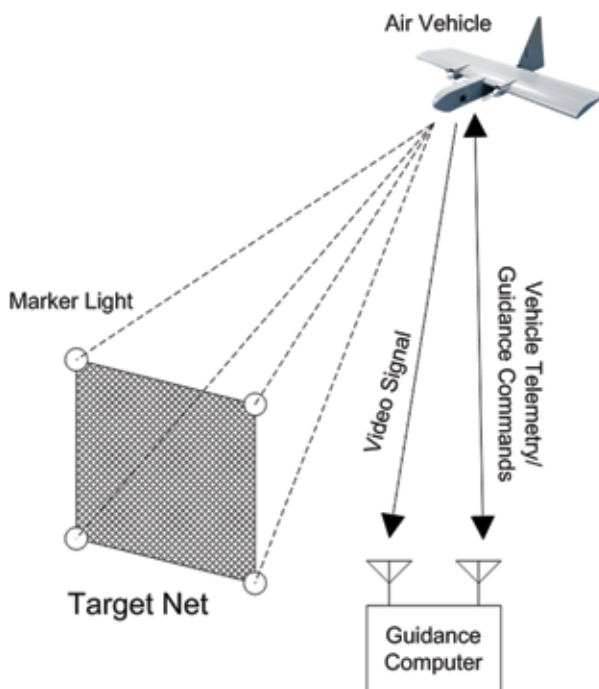
System Development: The development of the vision-based automatic landing system began with the creation of a simulation environment. The simula-tor models the behavior of the vehicle, autopilot, and data link, and generates a synthetic camera view. The simulation tool was useful in the invention and evaluation of the vision and guidance algorithms. In addition to computer simulation, a series of static real-world experiments were performed to validate the robustness of the machine vision algorithms in various lighting environments.

Flight experiments were conducted to evaluate the closed-loop performance of the prototype automatic landing system. The experiments were performed against a stationary optical landing target. The landing target was a square of 1.8 m per side with high-intensity lights at the corners. The vehicle was flown at a speed of approximately 18 m/s. With a camera resolution of 640×480 pixels and field of view of about 40 degrees, which is similar to that of cameras used on UAVs in current operation with the Fleet, the system can detect the landing target at a range of approximately 121 m. At this closure speed and range, the system has about 7 seconds to maneuver the vehicle into a collision path with the landing target. During the flight experiments, eight fully automatic approaches were performed, with the computer acquiring and tracking the target six times. Based on recorded video from the UAV, the vehicle would have hit the target on four attempts. This was estimated as the vehicle was told to automatically wave-off the approach at a range of 36.5 m from the target. This was done because the target was made of 2 by 4 lumber instead of a net. Figure 2 is a photograph of the UAV automatically approaching the target during one of these runs.

Conclusion: The new automatic recovery technology uses the existing hardware sensor package already present in many small tactical UAVs. The data from

these sensors are fused using a ship-based computer that generates steering commands for the vehicle to perform. This system has a significantly smaller footprint on board ship in comparison to other existing landing systems. Manpower requirements and logistics are reduced because the system performs recoveries fully automatically, and no additional expensive hardware is needed on board the air vehicle. A simulator was developed to evaluate the machine vision and guidance algorithms. A prototype system has been successfully flight tested.

References
[1] Sierra Nevada Corporation, "UCARS-V2: UAV Common Automatic Recovery System – Version 2 for Shipboard Operations," product brochure, 2006.
[2] The Insitu Group, Inc., "Unmanned System: Launch and Retrieval," http://www.insitu.com/launch_and_retrieval, 2010.
[3] RUAG, "Ranger UAV System," product brochure, 2006.

■

Simulating Natural Gas Explosions in Semiconfined Geometries

D.A. Kessler, V.N. Gamezo, and E.S. Oran
Laboratory for Computational Physics and Fluid Dynamics

Introduction: Detonations are violent, supersonic, high-pressure reaction waves that can develop during an explosion and cause severe damage. In the most powerful explosions, detonations can be initiated directly by strong shock waves. Under certain conditions, however, detonations can arise spontaneously from weak explosions or even from simple sparks.

This latter process, called the deflagration-to-detonation transition (DDT), takes place in two stages.[1] In the first stage, the relatively slow initial flame accelerates and becomes a fast, turbulent flame ("deflagration") that moves at nearly the speed of sound into the unburned but combustible gas. This can occur in semiconfined areas where the flow caused by thermal expansion of the burning gases acts like a piston to accelerate the flame. Flow instabilities and other interactions with the surrounding environment stretch and distort the flame and cause it to release energy more and more quickly. Eventually, pressure builds up in front of the flame and causes a high-pressure shock wave to form. In the second stage of the DDT process, this shock wave collides with physical obstructions or disturbances in the flow, heating and compressing small pockets of gas just ahead of the flame. The compressed gas in these "hot spots" can then ignite and produce a detonation.

In the past, this DDT process has been studied for simple, highly reactive fuels, such as hydrogen, acetylene, and ethylene. Now, we are working toward understanding the conditions necessary for DDT to occur in natural gas, an important but less reactive fuel that can be found in mine tunnels, access corridors on a ship, power-generation plants, fuel-storage facilities, and many other military and industrial settings. The loss of lives and property in several recent coal mine explosions in the United States and abroad have highlighted the need for an improved understanding of how and why detonations can form in natural gas explosions.

Model Development: Simulating an explosion requires specifying a model for the release of energy by chemical reactions in addition to solving the typical fluid flow equations. Detailed chemical models often involve hundreds of reactions. In a large, multidimensional simulation, computing each of these reactions would be too time-consuming. To make such computations feasible, we instead approximate the energy release from these hundreds of reactions with a single global reaction. This one-step model cannot exactly reproduce all properties of flames and detonations in natural gas–air mixtures, but we can calibrate it so that it gives reasonable approximations of the key length and time scales involved at the different stages of DDT, namely the speed, thickness, and temperature of flames and the speed and thickness of detonations in these mixtures.

Flame Acceleration and DDT in Semiconfined Channels: The calibrated reaction model is used with the usual fluid flow equations to simulate flame acceleration and DDT in a two-dimensional, semiconfined channel. The system we simulate, a diagram of which is shown in Fig. 3(a), is a simplified model of an experimental system that was used to study DDT in mixtures of methane (the primary fuel in natural gas) and air.[2] The physical obstructions arranged periodically in the channel help to more quickly accelerate the flame. A time progression of the temperature fields in the lower half of a 17.4 cm wide channel with obstructions blocking 30% of the cross-sectional area of the channel (blockage ratio of 0.3) is shown in Figs. 3(b-i). Both stages of the DDT process are shown. After being ignited by a weak spark, a flame travels from the closed (left) end of the channel toward the outflow. In the process, it becomes distorted and speeds up considerably.
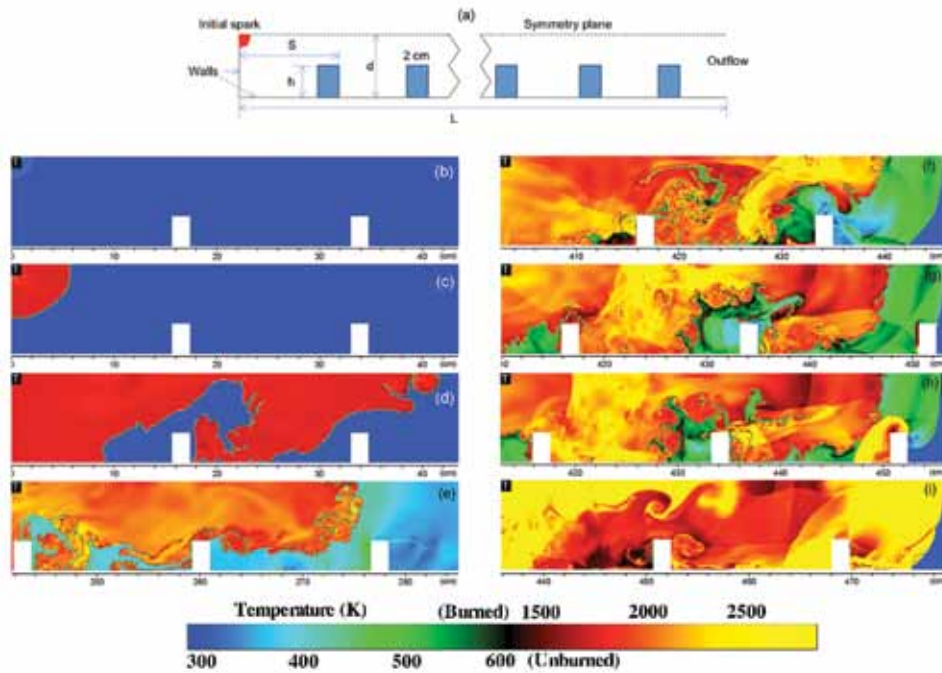
FIGURE 3
(a) Two-dimensional model geometry of a semiconfined space used in the simulations. Obstacles (blue rectangles) are spaced uniformly throughout the channels. We assume the channel is perfectly symmetric and simulate only the bottom half. In this simulation, d = 8.7 cm, h = 2.61 cm, L = 11.8 m, and S = 17.4 cm. (b-i) Temperature maps in the lower half of the channel near the leading edge of the reaction front showing (b) flame ignition by a weak spark, (c) laminar flame propagation, (d) flame stretching caused by thermal expansion and flame wrinkling, (e) pressure buildup in front of a deflagration, (f) shock wave formation, (g) hot spot formation after collision of a shock with an obstacle, (h) detonation initiation, and (i) detonation propagation.
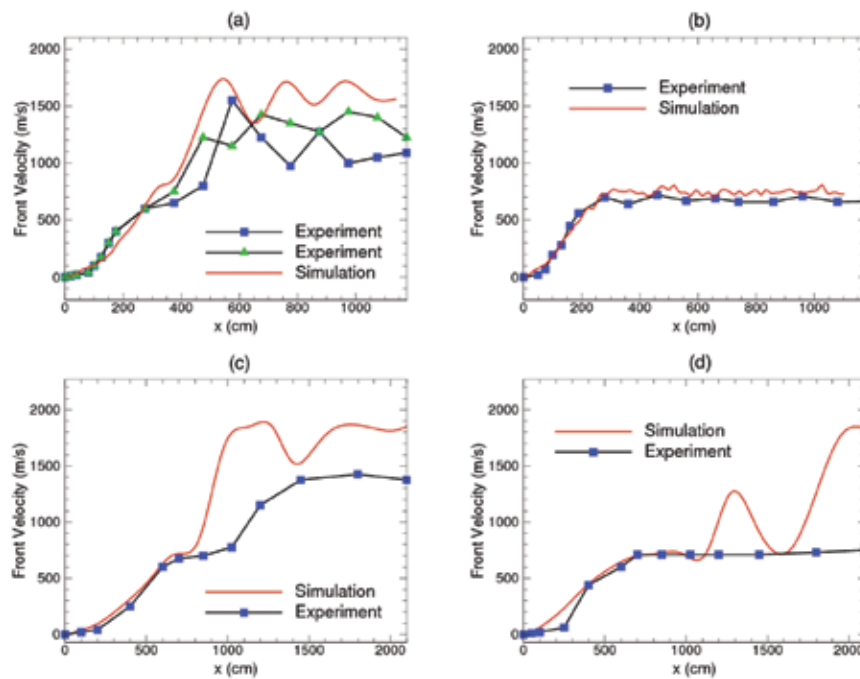

FIGURE 4
Velocity of the leading edge of the reaction front as a function of its position in the system calculated using the reaction model (red lines) and measured in experiments (blue and green symbols) for systems (a) 17.4 cm wide with blockage ratio 0.3, (b) 17.4 cm wide with blockage ratio 0.6, (c) 52 cm wide with blockage ratio 0.3, and (d) 52 cm wide with blockage ratio 0.6.

The shock wave that forms ahead of the flame collides with the solid obstacles, and the hot spot created by the collision shown in Fig. 3(g) ignites a detonation (see the figure caption and Ref. 3 for more complete descriptions). In Fig. 4(a), we compare the average velocity of the leading edge of the reaction zone in this simulation to several experimental measurements taken in a 17.4 cm diameter tube with the same blockage ratio. The results of three other simulations in channels of various sizes and blockage ratios are also compared to similar experiments in Figs. 4(b-d). The results calculated using the simple reaction model qualitatively, and in many cases quantitatively, match the experiments.

Summary and Future Directions: The innovation in this work is the development of a fast, reliable model for simulating DDT in natural gas–air mixtures that we have validated with existing experimental data. The speed of these calculations gives us the ability to simulate larger and more complex systems. We are currently working to understand how the DDT process scales to larger systems similar to those used in experiments conducted by the National Institute for Occupational Safety and Health (NIOSH)[4] and are finding that methane still detonates, in large systems, with concentrations lower than previously thought possible.

[Sponsored by NIOSH and NRL]

References
[1] E.S. Oran and V.N. Gamezo, "Origins of the Deflagration-to-Detonation Transition in Gas-Phase Combustion," *Combustion and Flame* **148**, 4–47 (2007).
[2] M. Kuznetsov et al., "DDT in Methane-Air Mixtures," *Shock Waves* **12**, 215–220 (2002).
[3] D.A. Kessler, V.N. Gamezo, and E.S. Oran, "Simulations of Flame Acceleration and Deflagration-to-Detonation Transitions in Methane-Air Systems," *Combustion and Flame* **157**, 2063–2077 (2010).
[4] R.K. Zipf, Jr., V.N. Gamezo, M.J. Sapko, W.P. Marchewka, K.M. Mohamed, E.S. Oran, D.A. Kessler, E.S. Weiss, J.D. Addis, F.A. Karnack, and D.D. Sellers, "Methane-Air Detonation Experiments at NIOSH Lake Lynn Laboratory," *Proceedings of the Eighth International Symposium on Hazards, Prevention, and Mitigation of Industrial Explosions, Yokohama, Japan, Sept. 5–10, 2010.*

Using Noise to Reveal Properties of Nonlinear Dynamical Systems: Making Noise Work for You

I.B. Schwartz,[1] L. Billings,[2] and M. Dykman[3]
[1] *Plasma Physics Division*
[2] *Montclair State University*
[3] *Michigan State University*

Introduction: In systems far from equilibrium, noise is found to play an increasingly important role in understanding the dynamics. Many of the systems we have studied, including delay coupled lasers,[1] adaptive networks,[2] and epidemic spread in finite populations,[3,4] are all modeled in the presence of noise. As sensing devices become smaller, or as the number of particles in populations gets smaller, new metastable states may be created, leading to novel observed dynamics.

For very small noise, it is known the system will remain close to an equilibrium state for very long times. However, if the system is nonlinear, sufficiently large noise will cause the system to leave its local attracting state, and explore other parts of phase space. In particular, it may find other distinct states, which may or may not be stable. If the dynamical system has more than one attracting state, noise may cause the dynamics to switch between states. A physical example of a system having more than one attractor is that of a micromechanical oscillator, shown in Fig. 5(a). It has a potential similar to that schematically drawn in Fig. 5(b), which is a generic picture of a bistable potential. It is clear that each attracting state is separated from the other by a barrier height of the potential, and in the case of
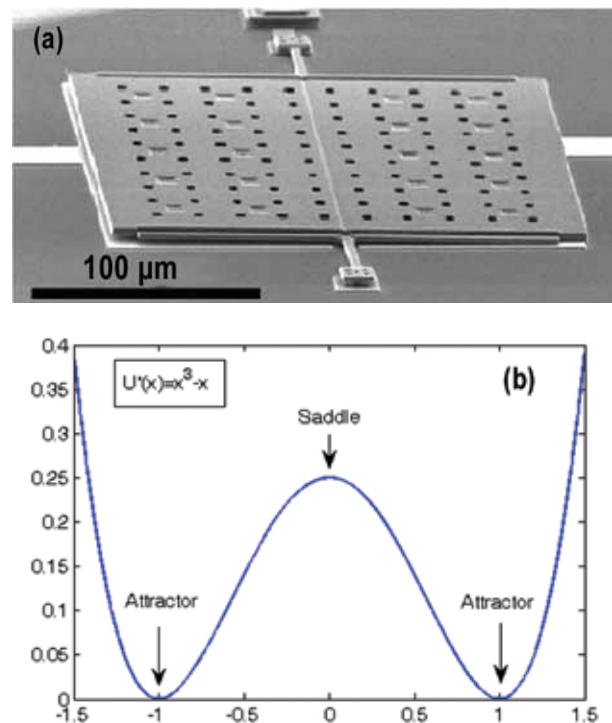

FIGURE 5
(a) An image of a micro-torsional oscillator. There are two stable states and hysteresis under suitable driving conditions. For details, see Ref. 8. (b) A schematic of a scalar potential possessing bistability. The two attracting states, located at the minima, are separated by an unstable object, such as a saddle. Deterministically, the trajectories go to one of the two attracting states, and remain there. However, if noise is added to the system, the trajectory may switch from one attractor to another.
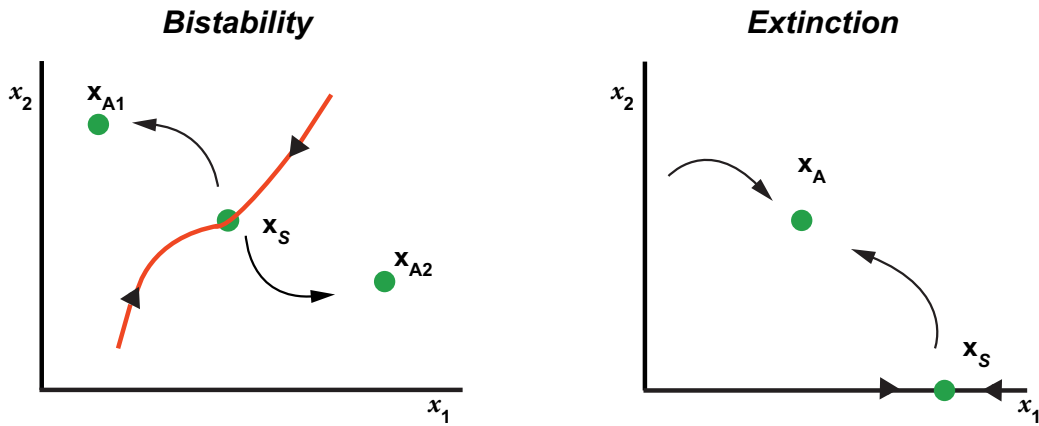
Bistability

Extinction

FIGURE 6
Phase portraits of two examples of changing states. (Left) The topology of a switching process. The stable manifold of a saddle divides the phase space between two attractors, forming a basin boundary. The stable manifold is a barrier that must be crossed in order to switch from one state to another. (Right) The topology of an extinction process. There exists a unique attracting state and an unstable extinct, which is a saddle. Noise drives the process to extinction by overcoming the unstable force of the extinct state.

Gaussian thermal noise, the exponent of the switching rate between attractors is proportional to the barrier height. The left graph in Fig. 6 depicts the phase space topology of the bistability in two dimensions. There is a saddle separating the two attracting states. The stable manifold acts as a basin boundary separating the basins of attraction between the two attractors. The noise must overcome the basin boundary to switch states.

On the other hand, if the system consists of a finite number of particles, such as a chemical reaction or population, noise may cause one or more of the species to approach zero, i.e., the species goes extinct. Generic epidemic models typically have one attracting endemic state and one extinct state. The extinct state is typically a saddle; the topology of this type of system is given in the right graph of Fig. 6. For extinction to occur, noise again must overcome an unstable barrier to approach the extinct state.

An example of probability to extinction is shown in Fig. 7(a). In this finite population epidemic model, there is one attracting state and one unstable extinct state. However, due to random interactions between
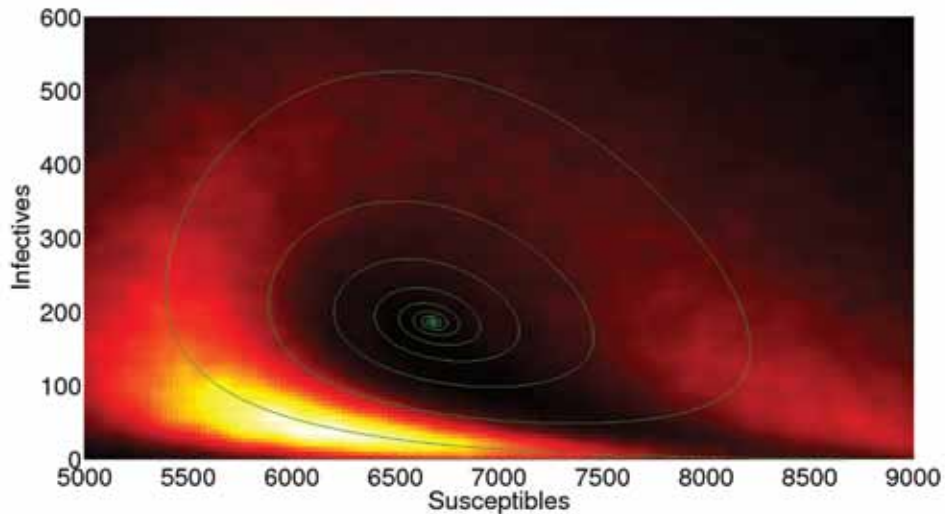

FIGURE 7(a)
An example of an extinction event in an epidemic model in a finite population of individuals. The population consists of infectious and susceptible individuals. Colors indicate the probability density (lighter corresponding to higher probability) for 20,000 stochastic realizations. The results were computed using Monte Carlo simulations. (Figure made by Simone Bianco, currently with the University of California at San Francisco.)
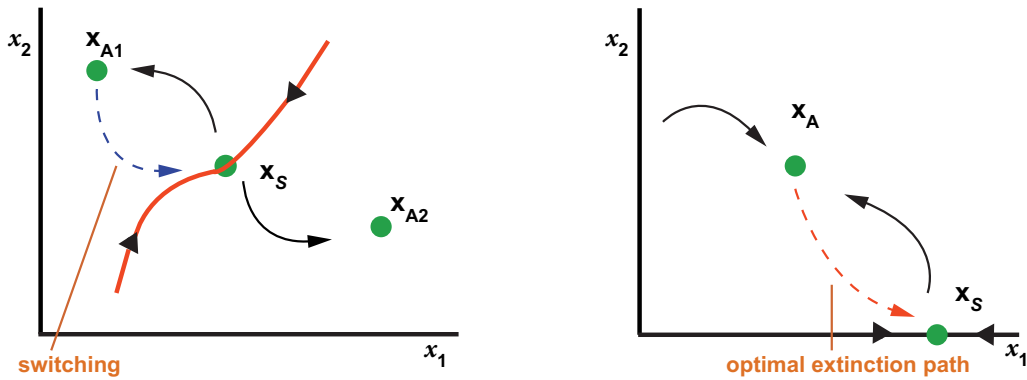
FIGURE 7(b)
A schematic of optimal paths for switching and extinction. (Left) The path to switch in a bistable situation. (Right) The optimal path to an extinct state. In both cases, noise is the driving force causing the system to overcome unstable directions of a saddle to either switch, as in the left panel, or go extinct.

particles, internal noise causes the system to overcome the instability of the extinct state, and one component vanishes.

One important point in understanding the probability of switching or extinction is that there exist many paths which generate a probability distribution of the events. One interesting question that may be asked is which paths optimize the probability of switching events, or extinctions? In particular, how do these paths arise as noise-driven events, and how do they depend on parameters of the system? The answers to these questions may be addressed by considering certain parameter regions. The graphs in Fig. 7(b) show possible optimal paths for switching and extinction, and the graph in Fig. 7(a) shows the actual optimal path for an epidemic model going from the endemic state to the extinct state where the number of infectious individuals (y-axis) approaches zero. For the rest of this article, we concentrate on quantifying switching rates in non-Gaussian noise situations near bifurcations. This is used to actually quantify parameters and noise characteristics in general sensing devices. References 5 through 7 provide the general theory in generic models as well as in stochastic models with multiple time scales.

Quantifying Switching Rates Near Instabilities: One aspect of nonlinear systems in noisy environments is that the rates of switching depend on a parameter that controls the number of states in the systems. In particular, when a system undergoes changes in stability or in the number of observed states in a system, it is said to undergo a bifurcation. Parameters ranges near bifurcations are important in that they control the rate at which the dynamics proceeds. In particular, the relevant components are slowed down in this range, and as a result of weak stability, noise-induced fluctuations are comparatively large. They ultimately lead to switching of the system from the stable state. Close to a bifurcation point, the switching rate becomes measurable even

where far from this point it is exceedingly small for a given noise level. The high sensitivity of the rate to the system parameters has been broadly used to determine parameters of many high quality sensing devices such as Josephson junctions and Josephson junction-based systems, nanomagnets, mechanical nanoresonators, and recently in quantum measurements. (Reference 5 provides a list of references to specific devices.)

The analysis of switching conventionally relies on the assumption that the underlying noise is Gaussian. Then the switching exponent Q, i.e., the exponent in the expression for the switching rate, $W \cong \exp(-Q)$, displays a power law dependence on the distance to the bifurcation point in the parameter space, η. That is, $Q = \eta^{\epsilon}$. Recently, there has been much interest in large fluctuations and switching induced by non-Gaussian noise. Such switching can be used to determine the noise statistics. However, the features of the switching rate near bifurcation points have not been explored. Yet, one may expect that the dependence of the switching exponent will differ from that for a Gaussian noise and will be very sensitive to the noise statistics. Indeed, we have found that there exists a non-power-law behavior when non-Gaussian noise is considered.

Non-Gaussian Noise-Induced Switching: We consider noise-induced switching in two different generic bifurcations: a saddle-node bifurcation and a pitchfork bifurcation. In both cases, we consider a Langevin problem where the potential function is a scalar, and the non-Gaussian noise source is Poisson, having amplitude *g* and mean frequency *v*. Figure 8 shows examples of two potential functions that characterize the saddle-node and pitchfork bifurcations. Several curves are plotted to illustrate the dependence on the bifurcation parameter for each bifurcation.

To predict what scaling law behavior occurs, we theoretically find the exponent of the switching rate. The exponent of the switching rate is given by classical
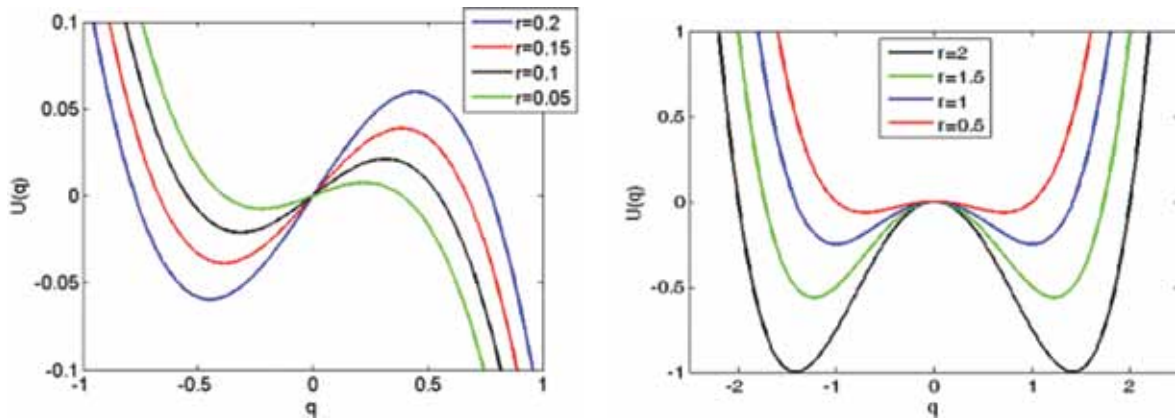
FIGURE 8
Potential functions for different bifurcation values of *r* in *U(q)*. The left panel is the potential for a saddle node bifurcation, while the right panel is that of a pitchfork bifurcation.
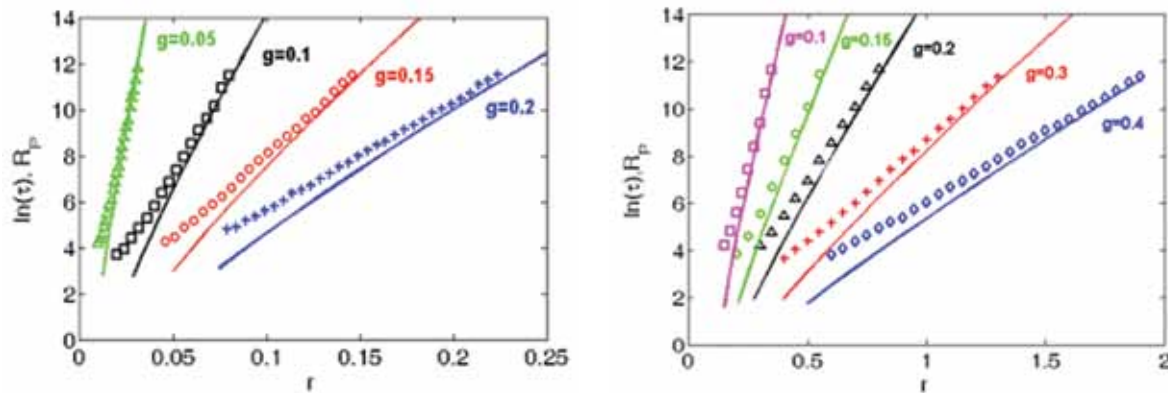

FIGURE 9
Switching exponents comparing numerical Monte Carlo simulations (symbols) vs theoretical predictions (solid curves). Poisson noise is characterized by amplitude *g* and mean frequency *v*. Pulses were only positive; i.e., pulses were one-sided. Saddle-node results are in the left panel and pitchfork results in the right panel.

analogue of the action, which is defined as the path integral from one state to the saddle. The trajectory of the path comes from an associated Hamiltonian, and may be computed from the derived equations of motion.

The interesting fact about computing the path for switching rates in a stochastic problem is that the optimal path maximizing the switching rate is determined by a deterministic conservative system. This system is twice the dimension of the original deterministic model. The extra dimensions model the noise as an effective force on the system, which drives the dynamics across the barrier. (See Fig. 7(a) for an optimal path example.)

The non-power-law behavior is predicted for both bifurcations in Ref. 5, and theory is compared with simulation in Fig. 9. Clearly, the power law dependence no longer exists due to a logarithmic correction. For Poisson noise, the change in sensor measurement characteristics is considerable, even for small noise amplitudes, *g*.

Conclusions: Many devices used as sensors, such as photonics and mesoscale devices, are driven by non-Gaussian noise sources. Here, we briefly reviewed new theoretical machinery that can characterize the physical parameters of a device by examining the scaling laws associated with switching rates. In contrast to power law behavior that is observed for Gaussian noise, non-Gaussian noise leads to non-power-law behavior. In the case of Poisson noise found in many devices, we find different logarithmic corrections in the two bifurcation scenarios. Thus, accurate measurements of switching rates may also determine the type of instability in the device, as well as where the bifurcation points are located.

Elsewhere, we have also considered the mixing between Gaussian and non-Gaussian sources.[5] It turned out that even a weak additional Gaussian noise becomes the major cause of switching sufficiently close to the bifurcation point. A qualitative and quantitative description of the crossover from Poisson- to Gaussian-

noise-controlled switching and of the bifurcation distance dependence of the switching exponent is in full agreement with numerical simulations.

[Sponsored by ONR]

References
[1] A.L. Franz, R. Roy, L.B. Shaw, and I.B. Schwartz, "Effect of Multiple Time Delays on Intensity Fluctuation Dynamics in Fiber Ring Lasers," *Phys. Rev. E* **78**(1), 016208 (2008).
[2] L.B. Shaw and I.B. Schwartz, "Enhanced Vaccine Control of Epidemics in Adaptive Networks," *Phys. Rev. E* **81**(4), 046120 (2010).
[3] I.B. Schwartz, L. Billings, M. Dykman, and A. Landsman, "Predicting Extinction Rates in Stochastic Epidemic Models," *J. Statistical Mechanics: Theory and Experiment* **2009**(1), P01005 (2009).
[4] E. Forgoston, S. Bianco, L.B. Shaw, and I.B. Schwartz, "Maximal Sensitive Dependence and the Optimal Path to Epidemic Extinction," *Bull. Mathematical Biol.*, **73**(3), 495–514 (2011).
[5] L. Billings, I.B. Schwartz, M. McCrary, A.N. Korotkov, and M.I. Dykman, "Switching Exponent Scaling near Bifurcation Points for Non-Gaussian Noise," *Phys. Rev. Lett.* **104**(14), 140601 (2010).
[6] E. Forgoston and I.B. Schwartz, "Escape Rates in a Stochastic Environment with Multiple Scales," *Siam J. Appl. Dynamic. Sys.* **8**(3), 119–1217 (2009).
[7] L. Billings, M.I. Dykman, and I.B. Schwartz, "Thermally Activated Switching in the Presence of Non-Gaussian Noise," *Phys. Rev. E* **78**(5), 051122 (2008).
[8] H.B. Chan, M.I. Dykman, and C. Stambaugh, "Paths for Fluctuation Induced Switching," *Phys. Rev. Lett.* **100**, 130602 (2008).

■